Dyes and Pigments 95 (2012) 1–7

Contents lists available at SciVerse ScienceDirect

Dyes and Pigments

journal homepage: www.elsevier.com/locate/dyepig

Electrical conductivity of carbon black pigments

Nina Hauptman [a,1], Alenka Vesel [b], Vladimir Ivanovski [c], Marta Klanjšek Gunde [a,*]

[a] National Institute of Chemistry, Hajdrihova 19, SI-1000 Ljubljana, Slovenia
[b] "Jožef Stefan" Institute, Jamova 39, SI-1000 Ljubljana, Slovenia
[c] Sts. Cyril and Methodius University, Faculty of Natural Sciences and Mathematics, Arhimedova 5, 1000 Skopje, Macedonia

ARTICLE INFO

Article history:
Received 18 January 2012
Received in revised form
9 March 2012
Accepted 13 March 2012
Available online 2 April 2012

Keywords:
Carbon black
Electrical conductivity
Particle size distribution
Raman spectroscopy
Infrared spectroscopy
X-ray photoelectron spectroscopy

ABSTRACT

The properties of carbon black surfaces which might affect their influence on the conductivity of dispersions in polar and non-polar media were analysed. Low-structured furnace black, high-structured gas black and extremely high-structured extra-conductive carbon black were studied. The size distribution of aggregates was measured. Raman spectroscopy provides relative amounts of disordered, graphitic and amorphous phases, and the lateral size of crystallites. X-ray photoelectron spectroscopy gives the oxygen content and the nature of functional groups on particle surfaces. The chemical nature of surface functional groups was analysed with infrared spectroscopy. All samples are disordered carbon blacks with different amounts of oxygen on their surfaces. The carbonyl-based surface groups were obtained on the acidic sample and other oxygen groups on the alkaline ones. A negligible amount of oxygen combined with a high amount of the graphitic phase and alkaline nature gives high conductivity of carbon black in polar and non-polar solvents. The conductivity of dispersion also increases with a higher structure, i.e. larger aggregates with a wide size distribution.

1. Introduction

Carbon black (CB) is one of the most useful carbon materials used in several products, e.g. tyres, plastics, electrostatic discharge compounds, pigmented coatings, toners and printing inks [1]. It contains at least 97% of carbon in grape-like cluster aggregates, the smallest indivisible CB units with various sizes, morphology, microstructure, surface chemistry and specific surface area [1]. The degree of aggregation is known as "structure". The extensive interlinking gives the so-called "high-structure" CB, while the less pronounced branching indicates the "low-structure" CB. The aggregates can be connected agglomerates which can be relatively easily broken. Smaller particles have better reinforcing capability in rubber and deeper colour in paints. When CB with larger aggregates are dispersed in an isolative polymer above the percolation threshold, the composite is electrically conductive. Such CBs are used in polymer composites for electromagnetic interference shielding [2], electrostatic discharge protection [3,4], conductive adhesives [5], for the sensing applications [6] and as conductive photoresists for electrically conductive micro-components [3,7].

The internal structure of primary particles consists of graphite-like crystalline and amorphous carbon domains. The graphitic phase is made of crystalline layers with lateral distances of a couple of nanometres while the amorphous one of polycyclic aromatic and other organic and inorganic compounds. The ratio of graphitic to amorphous phase depends on the starting materials and preparation conditions; the amount of graphitic phase is increased with annealing at high temperatures [1]. The surface chemical structure consists of groups with oxygen, nitrogen, hydrogen and/or sulfur, giving acidic or alkaline character in aqueous solution [8]. The overall basicity can also be attributed to the delocalized π-electrons in the basal planes of the CB structure [8].

The "structure" and surface chemical properties of CB particles affect the viscosity of liquid systems. The most effective polymer-adsorbing sites are at crystallite edges, whereas amorphous regions are less reactive. The reinforcing properties therefore depend on a fraction of the CB surface occupied by amorphous phase, on the size of crystallites and on their surface density [9]. The postproduction pressure treatment affects the size distribution of crystallites, while it essentially does not influence the average size of crystallites [10]. A different relative amount of amorphous carbon was detected on the CB surfaces with similar specific surface areas but no obvious influence on the surface activity was observed [11].

The impact of the aggregate surface chemical structure on electrical conductivity was studied by the internal conductivity of

* Corresponding author. Tel.: +386 1 4760200; fax: +386 1 4760300.
E-mail address: marta.k.gunde@ki.si (M.K. Gunde).
[1] Present address: Department of Molecular Genetics, Institute of Pathology, Medical Faculty, University of Ljubljana, Zaloška 4, SI-1000 Ljubljana, Slovenia.

0143-7208/$ – see front matter © 2012 Elsevier Ltd. All rights reserved.
doi:10.1016/j.dyepig.2012.03.012

thermal CB [12]. It was found to increase by decreasing the concentration of non-carbon elements, by increasing the poly-aromatic character and by decreasing the concentration of surface aliphatic groups. However, no correlation between the conductivity and bulk structure of CB was found. Somewhat different relationships were obtained for conductive CBs with a large specific surface area, where the conductivity strongly depends on the graphitic character of the surface, other surface properties having a very limited influence [13]. In these studies, electrical conductivity was measured with impedance spectroscopy on dried CB powder compressed between two metal plungers. The intrinsic conductivity measured this way also depends on the number of contacts among adjacent aggregates. The result of such measurements depends highly on compression pressure, sample volume, mechanical work and density of CB particles applied to prepare a homogeneous solid specimen [14]. Due to several possible contributions to conductivity, criteria were proposed to quantify the electrical conductivity of a moderately compressed carbonaceous powder [15].

In practice, CB particles are applied in a suitable medium. Recently, the CB powder has been used for the preparation of carbon-based conductive photoresist with percolation threshold of approx. 0.6 vol.% [7]. The negative near-UV sensitive epoxy-based photoresist was used as a polymer matrix [16]. The DC resistivity depends on the state of the CB dispersion and on the crosslinking of the polymer matrix. The composites with better dispersed particles showed up to one order of magnitude lower resistivity but crosslinking of the polymer matrix gives up to almost five orders of magnitude lower resistivity. The chemical properties of the interface between the polymer matrix and conductive fillers, as well as the influence of dispersing additive on this surface were studied [17]. The formation and the role of the interlayer between the CB particles and the host medium in a composite depend on their surface properties. The primary particle size and specific surface area, usually provided by the producer, are not sufficient to understand these phenomena. Therefore, the aim of the present study was to analyse and compare the surface properties of various CB types. Three forms of CBs, i.e. low-structured furnace black, high-structured high-colour gas black and extremely high-structured extra-conductive CB were analysed. The size of aggregates, the degree of structural order and the chemical properties on the particle surfaces were analysed. The results obtained for the three CB powders were compared and their role in the conductivity of dispersions in polar and non-polar media was discussed.

2. Materials and methods

Low-structured furnace black (Printex 200, pigment black), high-structured high-colour gas black (FW2, colour black) and extremely high-structured extra-conductive CB (XE2-B, extra-conductive black) were applied (Evonik Degussa, Germany). The average primary particle size (a) and specific surface area (BET) are given in Table 1.

Table 1
Average primary particle size (a) and BET surface area of analysed CB samples (producer's data).

Sample	Type	a (nm)	BET surface area (m^2/g)
Printex 200	pigment black	56	45
FW2	colour black	13	350
XE2-B	extra conductive black	30	1000

2.1. Conductivity and pH measurements

CB powder (0.40 g) was dispersed in Milli-Q water (40 mL) by the Hielscher UP400S ultrasonic processor at 40% power (160 W cm^{-2}) for 2 min. Another set of dispersions was prepared in the same way for the conductivity measurements in a non-polar medium (i.e. cyclohexane). Specific conductivity of dispersions was measured using the conductivity cell InLab 741 Conductivity Probe (Mettler Toledo) with the cell constant 0.1045 cm^{-1}. Three measurements were conducted consecutively to obtain the average value. The pH measurements were performed with the InLab Power Pro pH electrode (Mettler Toledo). The calibration of the electrode was performed with the buffer solutions at pH 4 and 7.

2.2. Light diffraction

The size distribution of aggregates was measured using a Malvern Particle Mastersizer 2000 laser diffraction apparatus. Each sample was ultrasonically treated to break the agglomerates. The particle size distributions were analysed with the average diameter (d_{av}), the peak value (d_{mode}), and with parameters describing the shape of the distribution: σ, k, and s are the standard deviation, kurtosis and skewness, respectively.

2.3. X-ray photoelectron spectroscopy (XPS)

The XPS spectra were recorded applying the TFA XPS Physical Electronics. The samples were excited with X-rays over a 400 μm spot area with the monochromatic Al $K_{\alpha 1,2}$ radiation at 1486.6 eV. Photoelectrons were detected with a hemispherical analyser at 45° with respect to the sample surface normal. The energy resolution was about 0.6 eV. The C1s survey scan spectra were made at the pass energy of 187.85 eV with the 0.4 eV energy step, while for carbon C1s, individual high-resolution spectra were taken at the pass energy of 23.5 eV with the 0.1 eV energy step. All spectra were analysed using the MultiPak v7.3.1 software (Physical Electronics). The energy scale was calibrated according to the C1s (C–C) peak, which was shifted to 284.5 eV and is typical of graphite [18,19]. A Shirley-type background subtraction was used. The elemental composition of the surface was evaluated using the relative sensitivity factors from the manufacturer's handbook.

2.4. Raman spectroscopy

Raman spectroscopy was used to identify crystalline, amorphous and disordered phases [20–24]. The most prominent peak is the ideal graphitic lattice mode with the E_{2g} symmetry at about 1582 cm^{-1}, called the G-peak (graphitic). In disordered structures this band broadens; four additional D-bands (disordered) may appear at about 1340, 1620, 1510 and 1180 cm^{-1}, called D1, D2, D3 and D4, respectively. The strong D1 band is caused by symmetric C–C vibrations of structural defects in graphitic layers. Its intensity decreases by the size of graphitic planes. The D2 band is a weak shoulder at the G-mode. The medium-intense D3 band shows the presence of the amorphous phase and is also denoted the A-band (amorphous). D4 is a weak band originated by C=C stretching vibrations in the disordered graphitic lattice. When crystallinity increases, the G-peak increases with respect to D1, both G and D1 peaks become narrower and move towards higher wavenumbers [9,10]. The second order Raman spectrum consists of overtones and combinations of graphitic lattice vibrational modes [24].

The Raman spectra of all CB powders were recorded using micro Raman system (LabRAM 300, Horiba Jobin-Yvon) at the excitation of 532 nm (Nd:YAG) in the 100 cm^{-1} to 4000 cm^{-1} region with

resolution between 3 and 4 cm^{-1}. Filter adjustments and acquisition times were set for each sample separately to avoid burning.

The overlapping peaks in the first and second order Raman spectra were resolved into Lorentzian or Gaussian peak shapes, using the GRAMS/32 (Galactic Industries Corporation) software program. The goodness-of-fit was evaluated with the reduced χ^2, which approached unity when a perfect fit was obtained. The relative amounts of the graphitic, disordered and amorphous phase were expressed by the area portion occupied by the corresponding peak in the entire first order Raman spectrum. The first and the second order Raman spectra of each studied sample were fitted separately and independently.

The lateral size of crystallites (L_a) was calculated according to the equation [9,20]:

$$\mathrm{La} = 4.35 \cdot I(G)/I(D1), \quad (\text{in nm}) \tag{1}$$

where I(G) and I(D1) represent the intensity of G and D1 modes, respectively.

2.5. IR spectroscopy

The IR spectra of CB samples are difficult to obtain due to the problems in the sample preparation, high overall absorbance and size-dependent scattering [25,26]. Their interpretation is not straightforward, while individual functional groups may appear in a wide range of different electronic environments giving broad bands with low intensity on a very high overall absorbance [25–27].

The IR spectra of CB samples were recorded carefully using the Bruker Spectrometer IFS 66/S in the transmission mode. Each powder was mixed with KBr and pressed into pellets for recording. The final absorbance spectra were baseline-corrected.

3. Results and discussion

3.1. Conductivity and pH

All powders sank almost immediately into cyclohexane when placed on its surface but behave differently on surface of water. In such experiment, the XE2-B powder floated on the surface of water for a longer period of time, pointing to more hydrophobic nature, but Printex 200 and FW2 sank faster due to a more hydrophilic nature of their surfaces.

The pH values and conductivity are given in Table 2. The FW2 has acidic character, whereas Printex 200 and XE2-B are mildly alkaline. Different conductivity was obtained for the CB samples dispersed in water and cyclohexane solvents, the highest for the XE2-B sample.

The conductivity of CB dispersions is related not only to the intrinsic conductivity of particles, but also to the particle properties in the applied solvent. If larger particle clusters tend to be formed, an electric charge through the dispersion is promoted. This could be seen at the XE2-B sample which had conductivity two times higher in water than in cyclohexane. In a polar solvent the conductivity is correlated with the specific surface area: the larger the BET area, the higher the conductivity. The effect is much smaller in cyclohexane, the corresponding conductivity thus being lower.

Table 2
Measured pH values and conductivity of CB dispersions in polar (water) and non-polar (cyclohexane) solvents.

Sample	pH (1 ± 0.02)	Conductivity (μS/cm)	
		H_2O	Cyclohexane (1 ± 0.01)
Printex 200	7.5	12 (1 ± 0.04)	70
FW2	3.1	430 (1 ± 0.11)	69
XE2-B	8.0	1370 (1 ± 0.10)	720

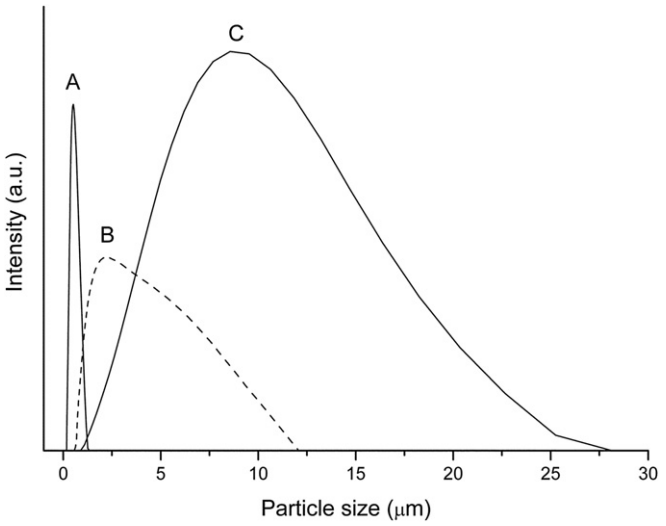

Fig. 1. Size distribution of aggregates in Printex 200 (A), FW2 (B) and XE2-B (C) samples as measured by laser diffraction. Corresponding parameters are given in Table 3.

3.2. Particle size distribution

The measured particle size distributions are shown in Fig. 1. The Printex 200 has the smallest particles and the XE2-B the largest. The size distributions are non-Gaussian and right-skewed (Table 3). Each of the three size distribution graphs peaks at a lower value than the average size (d_{av}). The effect is evaluated with skewness (s), which is the largest in the FW2 sample and the smallest in the Printex 200. The Printex 200 has the smallest variation of particle sizes; the standard deviation (σ) is about 10 times larger for the FW2 sample and more than 20 times larger for XE2-B. Both diameters of aggregates, the average (d_{av}) and mean (d_{mode}), increase with the BET surface area.

3.3. XPS spectra

The XPS survey spectra of all three samples are shown in Fig. 2. Some oxygen was found: about 10 at.% in FW2 sample, somewhat lower in Printex 200, while in XE2-B, only small traces of oxygen were found (below 1 at.%).

The chemical state of carbon was determined from the high-resolution carbon spectra (Fig. 3). They show the presence of new peaks for two samples with higher oxygen content. In the sample Printex 200, the oxygen is bound mostly in the C–O groups, while in the sample FW2, the oxygen is preferable in the O=C–O groups. This result corresponds well to the pH values (cf. Table 2): the FW2 sample with acidic nature has oxygen in the acidic O=C–O surface groups and the alkaline Printex 200 in the non-acidic C–O groups.

Table 3
Characteristic parameters of size distribution graphs (cf. Fig. 1): average diameter (d_{av}), mean diameter (d_{mode}), standard deviation (σ), kurtosis (k) and skewness (s).

Sample	d_{av} (μm)	d_{mode} (μm)	σ (μm)	k	s
Printex 200	0.53	0.51	0.21	2.9	0.7
FW2	3.35	2.27	2.19	3.4	1.1
XE2-B	8.66	8.56	4.74	3.3	0.8

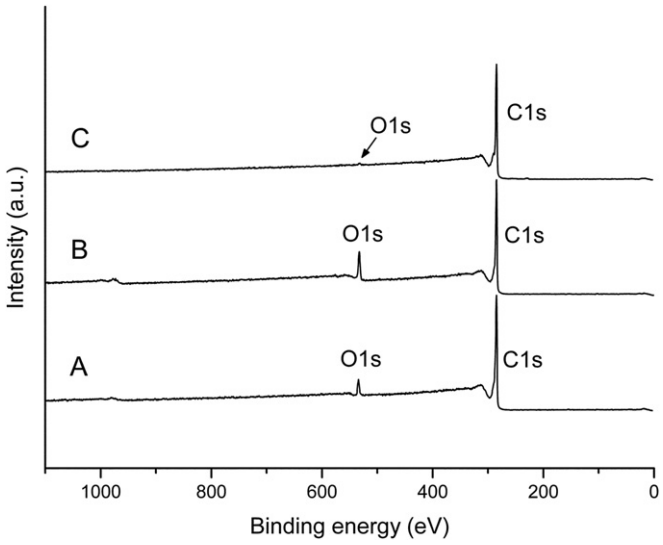

Fig. 2. XPS survey spectra of Printex 200 (A), FW2 (B) and XE2-B (C) samples.

The C1s peak of the XE2-B sample is very narrow (FWHM = 0.85 eV), while the C1s peaks for Printex 200 and FW2 are wider with FWHM = 1.0 and 1.1 eV, respectively. The intensity of π-satellites of these two samples is much weaker as for the XE2-B sample, suggesting that the character of the XE2-B sample is more graphitic than of the other two. This result is also in agreement with the results obtained from the Raman spectroscopy [28,29].

3.4. Raman spectra

The first order Raman spectra of all three samples are shown in Fig. 4. Two strong peaks (G and D1) and two weak peaks (D3 and D4) are present. While no shoulder of the G mode was obtained the

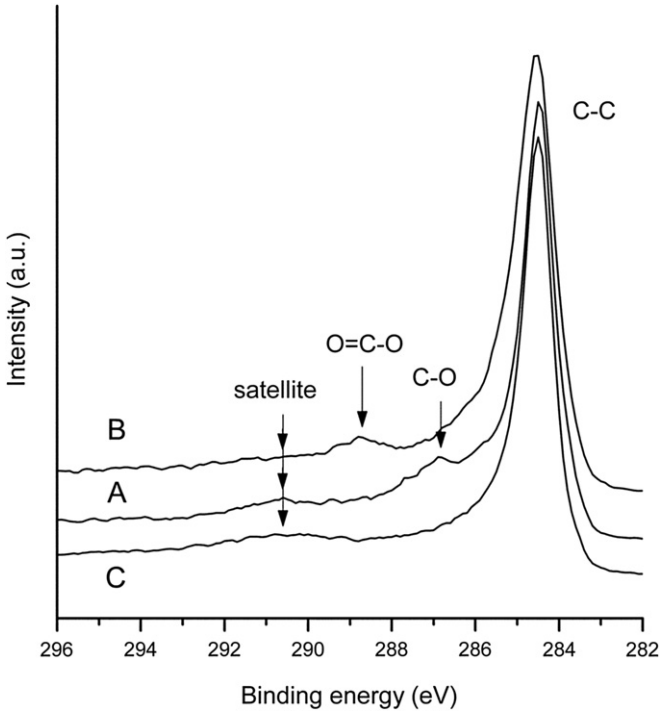

Fig. 3. XPS C1s spectra of Printex 200 (A), FW2 (B) and XE2-B (C) samples showing different carbon-oxygen bonds and $\pi \rightarrow \pi^*$ satellite bands.

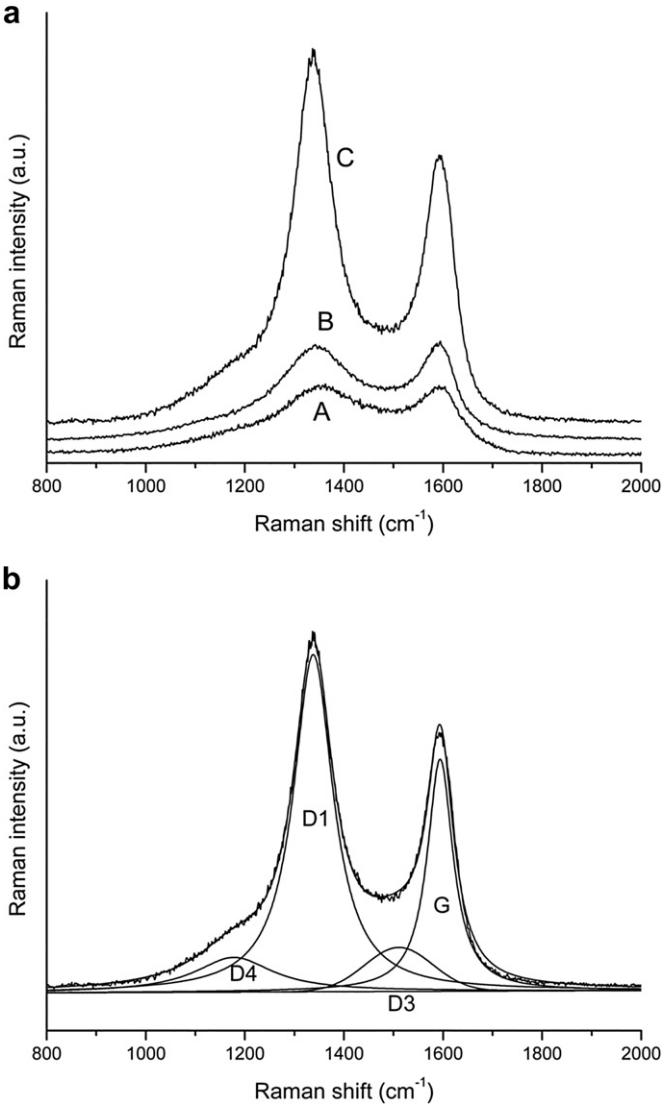

Fig. 4. First order Raman spectra of Printex 200 (A), FW2 (B) and XE2-B (C) samples, (a), and results of spectral analysis for sample XE2-B with D1, G, D3 and D4 peaks, (b).

D2 peak was not taken into account in analysis (Fig. 4b, Table 4). The D3 peak has purely Gaussian lineshape whereas all others purely Lorentzian. The goodness-of-fit (the reduced χ^2) was below 1.7 for all three spectra.

The two strong peaks (G and D1) were obtained at approximately the same position in all samples showing similar crystallinity. Larger differences were observed in the positions of the D3 and D4 mode. The D3 peak shows the presence of fragments or functional groups in the amorphous phase which may also change the C—C and C=C stretching vibrations of the polyene-like structure (D4). Therefore, these molecular species differ among the three samples. The width of the G peak slightly decreases with the BET surface area of the sample.

The lateral sizes of crystallites, L_a, were calculated applying Eq. (1) (Table 4). Lower values were obtained for the sample with smaller aggregates.

The area portion obtained for the G, D1 and D3 peaks evaluate the relative content of graphitic, disordered and amorphous phases, respectively. The most intensive is the D1 peak; it occupies more than 45% area of the first order structure, the largest in the FW2 sample. This correlates with the primary particle sizes (cf. Table 1):

Table 4
Data for four resolved peaks in first order Raman spectra: position (ν_0), relative intensity (I_0), full-width at half height (FWHH) and corresponding area portion. Relative intensity gives the intensity ratio of the corresponding band and D1 band. L_a is the size of crystallites. The area portion of G, D1 and D3 peaks evaluates the relative content of graphitic, disordered and amorphous phases, respectively.

Mode	Printex 200				FW2				XE2-B			
	ν_0 (cm^{-1})	I_0	FWHH (cm^{-1})	Area (%)	ν_0 (cm^{-1})	I_0	FWHH (cm^{-1})	Area (%)	ν_0 (cm^{-1})	I_0	FWHH (cm^{-1})	Area (%)
D4	1189	0.251	240	16	1142	0.104	254	9	1178	0.103	191	11
D1	1346	1	171	47	1344	1	187	62	1338	1	97	56
D3	1498	0.397	208	17	1529	0.251	152	9	1511	0.131	161	8
G	1597	0.879	82	20	1594	0.815	71	20	1594	0.689	63	25
L_a (nm)	3.5				3.8				3.0			

the sample with larger primary particles has a smaller amount of the disordered phase. However, a smaller amount of the disordered phase is not necessarily accompanied by a higher amount of the graphitic phase.

The second order Raman spectra are shown in Fig. 5. The assignment of peaks was obtained by combining the positions of the first order Raman bands (Table 5). They involve at least one intense band (D1 or G): three combinations (D1 + G), (D1 + D4) and (G + D3) and the first overtone of D1 (2D1). This confirms that the D2 band is not excited in our samples.

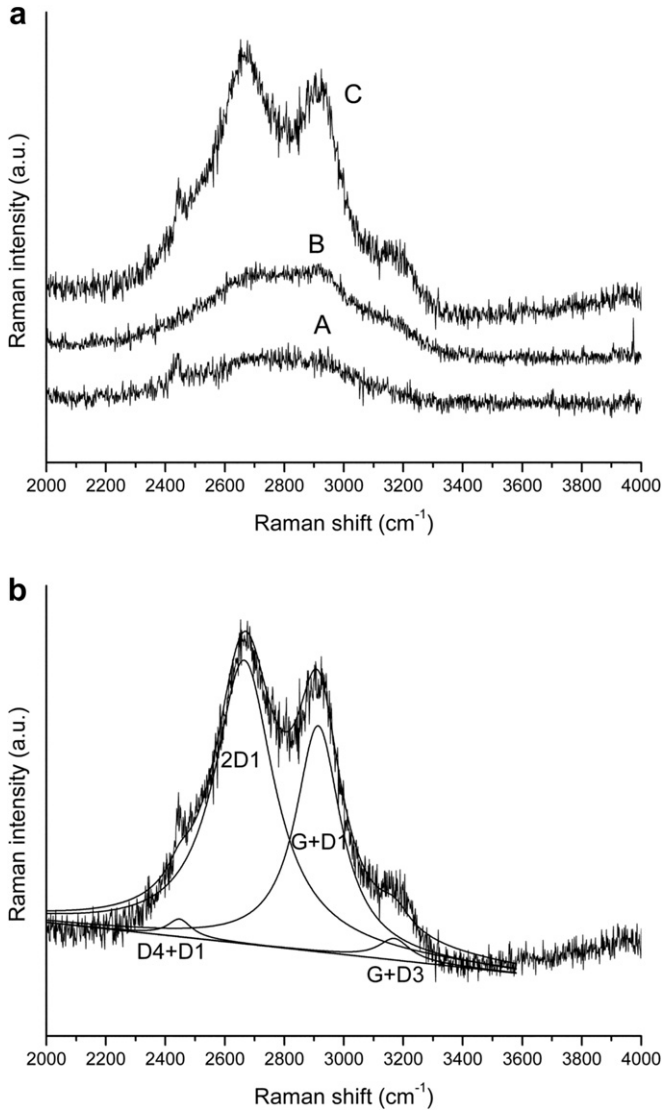

Fig. 5. Second order Raman spectra of Printex 200 (A), FW2 (B) and XE2-B (C) samples, (a), and result of spectral analysis for XE2-B sample, (b).

3.5. IR spectra

The IR spectra of the three CB powders are shown in Fig. 6. Three broad peaks were obtained, i.e. at 1740, at about 1600 and at 1260 cm^{-1}. The peak at 1740 cm^{-1} appears only in the FW2 sample. It originates from the carbonyl (C=O) stretching vibrations [26]. The second broad peak appears in all samples at around 1600 cm^{-1}. It could originate from the asymmetrical stretching of the aromatic C=C bond reinforced by some oxygen atoms near one of the vibrating C atoms [30–32]. This suits well to the vibration of the C-ring with the zigzag phenol groups at 1590 cm^{-1} as calculated for the polyaromatic model system [26]. A similar intensity and position of this peak was obtained for the FW2 and Printex 200 samples. It was reported that simultaneous existence of the carbonyl band may appear in polyaromatic systems with both the cyclic ketone and ether rings on the CB surface [8,26] which was observed on FW2 sample. According to the XPS results, the XE2-B sample has negligible oxygen content. Therefore, a broad peak located at approximately 1580 cm^{-1} cannot reveal any oxygen-attended vibration, but corresponds well with the E_{1u} mode of the graphitic crystal lattice which is IR active and should appear at 1590 cm^{-1} [21]. The existence of this peak shows a pronounced presence of the graphitic structure in the XE2-B sample. The third peak at about 1250 cm^{-1} could be attributed to different functional groups such as C–C and C–O–C stretching and C–H deformation of the aromatic hydroxyl unit that is hydrogen-bonded to the conjugated carbonyl group [30,31]. This peak is best pronounced in the FW2 sample and could be almost neglected in the XE2-B sample.

Different behaviour of CB powders in a polar solvent could be understood with the combined effect of the specific surface area, aggregate size and surface chemical properties. The amount of the graphitic phase (from Raman) correlated well with the width of the C1s peak in the XPS spectra. The sample with the highest amount of the graphitic phase and practically no oxygen had IR peak at about 1580 cm^{-1} due to the graphitic crystal lattice vibration and no peaks due to the oxygen-containing functional groups. The IR spectra confirm that the carbonyl-based surface groups exist only

Table 5
Data for four peaks in the second order Raman spectra of three samples: position (ν_0), intensity (I_0, ratio of Raman intensities of corresponding band and that of D1 band obtained for the same sample) and most suitable assignment (mode).

Mode	Printex 200			FW2			XE2-B		
	ν_0 (cm^{-1})	I_0	Area (%)	ν_0 (cm^{-1})	I_0	Area (%)	ν_0 (cm^{-1})	I_0	Area (%)
D4 + D1	2441	0.042	6	2524	0.019	9	2448	0.005	2
2·D1	2699	0.088	68	2696	0.085	47	2665	0.085	59
G + D1	2929	0.050	23	2923	0.088	39	2914	0.068	37
G + D3	3030	0.007	3	3149	0.024	5	3171	0.006	2

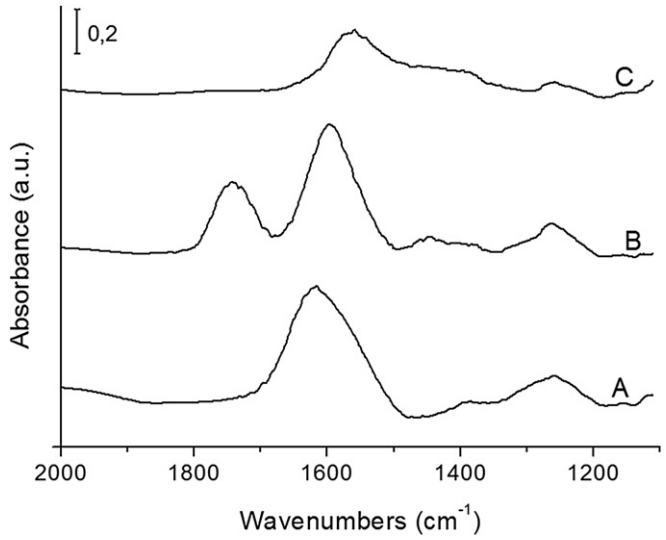

Fig. 6. IR spectra of Printex 200 (A), FW2 (B) and XE2-B (C) samples.

on an acidic CB surface, whereas on an alkaline surface, other oxygen groups (phenol and C–O–C) are preferred.

The conductivity of the investigated dispersions is higher in a polar medium and lower in a non-polar one, which is valid for the particles with a smaller amount of the amorphous phase. A higher amount of the graphitic phase combined with the alkaline nature and a negligible amount of the surface groups is the most important for the highest conductivity in the polar and non-polar media.

4. Conclusions

On the investigated carbon black pigments the disordered phase prevails over the graphitic and amorphous ones. The average diameter of aggregates wax found well below μm in low structured samples and over 8.5 μm in high structured ones, whereas the width of corresponding size distributions was found to be about 0.2 and 4.7 μm, respectively. This shows a large extent of random branching between primary particles.

The analysed samples have a different amount of surface oxygen, which disturbs the graphitic phase on the particle surfaces. The extra-conductive sample has practically no oxygen bonded on the large, extremely high-structured aggregates. These aggregates have the largest content of the graphitic crystal form and the smallest lateral sizes of crystallites.

Only the compound with extremely high-structured aggregates and with the highest graphitic phase content gives conductive polymer composites. Their conductivity depends also on the structure of the polymer matrix [7]. The polarity of the applied solvent plays an important role in the conductivity of dispersions, which could be understood with the combined effect of the specific surface area, aggregate size and surface chemical properties. The ability of carbon black particles to form chemical bonds between the surface and the additive highly supports the conductivity of the final composite. Stronger bonds are formed on the surface with less oxygen, which promotes the electric charge flow [17].

The major factor that determines the electrical conductivity of carbon black particles is the graphitic character giving delocalized π-electrons. The chemical structure on the particle surfaces influences the electrical conductivity of the dispersion by enabling chemical bonds between the particle and the medium. The structure and size distribution of aggregates additionally promotes the conductivity. All these factors influence the conductivity of the final application.

Acknowledgements

The authors would acknowledge the financial support from the state budget by the Slovenian Research Agency (project No. J2-9455). Nina Hauptman acknowledges the Slovenian Research Agency for the young researchers support. The authors express their gratitude to Evonik Degussa d. o. o. in Croatia for the provided CB samples and support.

References

[1] Donnet JB, Bansal RC, Wang MJ. Carbon black: science and technology. New York: Marcel Dekker; 1993.
[2] Strümpler R, Glatz-Reichenbach J. Conducting polymer composites. J Electroceram 1999;3:329–46.
[3] Im JS, Kim JG, Lee Y-S. Fluorination effects of carbon black additives for electrical properties and EMI shielding efficiency by improved dispersion and adhesion. Carbon 2009;47:2640–7.
[4] Chung DDL. Electrical applications of carbon materials. J Mater Sci 2004;39:2645–61.
[5] Li Y, Wong CP. Recent advances of conductive adhesives as a lead-free alternative in electronic packaging: materials, processing, reliability and applications. Mater Sci Engn 2006;R51:1–35.
[6] Flandin L, Bréchet Y, Cavaillé J-Y. Electrically conductive polymer nanocomposites as deformation sensors. Compos Sci Technol 2001;61:895–901.
[7] Hauptman N, Žveglič M, Maček M, Klanjšek Gunde M. Carbon based conductive photoresist. J Mater Sci 2009;44:4625–32.
[8] Montes-Morán MA, Suárez D, Menéndez JA, Fuente E. On the nature of basic sites on carbon black surfaces: an overview. Carbon 2004;42:1219–25.
[9] Ungár T, Gubicza J, Tichy G, Pantea C, Zerda TW. Size and shape of crystallites and internal stresses in carbon blacks. Composites Part A 2005;36:431–6.
[10] Ungár T, Gubicza J, Ribárik G, Pantea C, Zerda TW. Microstructure of carbon blacks determined by X-ray diffraction profile analysis. Carbon 2002;40:929–37.
[11] Tricás N, Vidal-Escales E, Borrós S, Gerspacher M. Influence of carbon black amorphous phase content on rubber filled compounds. Compos Sci Technol 2003;63:1155–9.
[12] Pantea D, Darmstadt H, Kaliaguine S, Sümmchen L, Roy C. Electrical conductivity of thermal blacks: influence of surface chemistry. Carbon 2001;39:1147–58.
[13] Pantea D, Darmstadt H, Kaliaguine S, Roy C. Electrical conductivity of conductive carbon blacks: influence of surface chemistry and topology. Appl Surf Sci 2003;217:181–93.
[14] Sánchez-González J, Macías-García A, Alexandre-Franco MF, Gómez-Serrano V. Electrical conductivity of carbon blacks under compression. Carbon 2005;43:741–7.
[15] Celzard A, Mareché JF, Payot F, Furdin G. Electrical conductivity of carbonaceous powders. Carbon 2002;40:2801–15.
[16] Klanjšek Gunde M, Hauptman N, Maček M, Kunaver M. The influence of hard-baking temperature applied for SU8 sensor layer on the sensitivity of capacitive chemical sensor. Appl Phys A 2009;95:673–80.
[17] Hauptman N, Klanjšek Gunde M, Kunaver M, Bešter-Rogač M. Influence of dispersing additives on the conductivity of carbon black pigment dispersion. J Coat Technol Res 2011;8:553–62. doi:10.1007/s11998-011-9330-5.
[18] Moulder JF, Stickle WF, Sobol PE, Bomben KD. Standard XPS spectra of the elements. In: Chastain J, King RC, editors. Handbook of X-ray photoelectron spectroscopy. Minnesota: Physical Electronics Inc.; 1995. p. 40–253.
[19] Hontoria-Lucas C, López-Peinado AJ, López-Gonzáles JD, Rojas-Cervantes ML, Martin-Aranda RM. Study of oxygen-containing groups in a series of graphite oxides: physical and chemical characterization. Carbon 1995;33:1585–92.
[20] Tuinstra F, Koenig JL. Raman spectrum of graphite. J Chem Phys 1970;53:1126–30.
[21] Wang Y, Alsmeyer DC, McCreery RL. Raman spectroscopy of carbon materials: structural basis of observed spectra. Chem Mater 1990;2:557–63.
[22] Cuesta A, Dhamelincourt P, Laureyns J, Martínez-Alonzo A, Tascón JMD. Raman microprobe studies on carbon materials. Carbon 1994;32:1523–32.
[23] Jawhari T, Roid A, Casado J. Raman spectroscopic characterization of some commercially available carbon black materials. Carbon 1995;33:1561–5.
[24] Sadezky A, Muckenhuber H, Groethe H, Niessner R, Pöschl U. Raman microspectroscopy of soot and related carbonaceous materials: spectral analysis and structural information. Carbon 2005;43:1731–42.
[25] Rositani F, Antonucci PL, Minutoli M, Giordano N, Villari A. Infrared analysis of carbon blacks. Carbon 1987;25:325–32.
[26] Fuente E, Menéndez JA, Díez MA, Suárez D, Montes-Morán MA. Infrared spectroscopy of carbon materials: a quantum chemical study of model compounds. J Phys Chem B 2003;107:6350–9.
[27] Llamas-Jansa I, Jäger C, Mutschke H, Henning Th. Far-ultraviolet to near-infrared optical properties of carbon nanoparticles produced by pulsed-laser pyrolysis of hydrocarbons and their relation with structural variations. Carbon 2007;45:1542–57.
[28] Leiro JA, Heinonen MH, Laiho T, Batirev IG. Core-level XPS spectra of fullerene, highly oriented pyrolitic graphite, and glassy carbon. J Electron Spectrosc Relat Phenom 2003;128:205–13.

[29] Briggs D. Surface analysis of polymers by XPS and static SIMS. Cambridge: Cambridge University Press; 2005.
[30] Colthup NB, Daily LH, Wiberley SE. Introduction to infrared and Raman spectroscopy. Boston: Academic Press; 1990.
[31] Boehm HP. Surface oxides on carbon and their analysis: a critical assessment. Carbon 2002;40:145–9.
[32] Jäger C, Henning Th, Schlögl R, Spillecke O. Spectral properties of carbon black. J Non-Cryst Solids 1999;258:161–79.